Topological superradiance in a shaken dynamical optical lattice

Yanlin Feng, Jingtao Fan, Xiaofan Zhou, Gang Chen,* and Suotang Jia
State Key Laboratory of Quantum Optics and Quantum Optics Devices, Institute of Laser Spectroscopy, Shanxi University, Taiyuan, Shanxi 030006, China
and Collaborative Innovation Center of Extreme Optics, Shanxi University, Taiyuan, Shanxi 030006, China

(Received 22 November 2018; published 29 April 2019)

In the present paper, we consider the steady state of Fermi atoms coupled to a shaken cavity field at half filling. This shaking generates a time-dependent dynamical optical lattice with backaction on the atomic degrees of freedom. In the high-frequency limit, the shaken dynamical optical lattice produces interesting cavity-field-dependent long-range hoppings, including the nearest-, next-nearest-, and next-next-nearest-neighbor hoppings. They can change the band structures of the system and thus induce nontrivial topological superradiant phases, especially with a large winding number and four degenerate edge states. We also briefly address possible experimental observations of the predicted topological superradiant phases. Our results provide an alternative way to explore novel many-body physics in cavity quantum electrodynamics systems.

DOI: 10.1103/PhysRevA.99.043630

I. INTRODUCTION

The interplay of ultracold atoms and a high-finesse optical cavity has recently attracted much attention, since this system is a powerful platform to process quantum information and explore exotic many-body phenomena [1]. A key feature of such system is that the ultracold atoms can self-organize into a dynamical optical lattice potential induced by the coherent cavity field, and in turn affect the light scattering into the cavity [2–14]. Another is that the cavity field can act as a medium that induces a global long-range interaction between ultracold atoms. When it competes with the short-range interaction, rich quantum phase transitions, such as the supersolid [15–24] and magnetic [25,26] phase transitions, can occur. The cavity field can also generate gauge potentials and thus produces topological superradiant states [27,28].

On the other hand, the shaking provides an additional way for the coherent manipulation of many-body systems [29]. In particular, the ultracold atoms in the shaken optical lattices open up a new avenue for studying Floquet physics [30–44]. These previous studies are almost based on the fact that the parameter modulations are determined solely by the external shaking and are independent of the system dynamics. In fact, this shaking technique can also be well realized in an optical cavity through the electro-optic modulators of the cavity mode. In such a case, the shaken optical lattice is however dynamical; i.e., the Floquet dynamics and the parameter modulations are mutually dependent, generating exotic many-body phenomena. For example, a self-adapted Floquet dynamics has been found, which exhibits two unique features: the phase transition from the normal to the superradiant phases has a hysteresis even without the atomic interaction and the dynamical atom-cavity steady state could exist at free-energy maxima [45]. In this paper, we mainly use this shaking technique to achieve rich cavity-field-dependent long-range hoppings in a dynamical optical lattice. These long-range hoppings can change the band structures of the system and then induce nontrivial topological superradiant phases with large winding numbers.

Specifically, we consider the steady state of the Fermi atoms coupled to a shaken cavity field at half filling. This shaking of the cavity field generates a time-dependent dynamical optical lattice with backaction on the atomic degrees of freedom. In the high-frequency limit, the cavity-field-dependent long-range hoppings, including the nearest- (NN), next-nearest- (NNN), and next-next-nearest-neighbor (NNNN) hoppings, are realized with high controllability. By self-consistently calculating the bulk property under the periodic boundary condition, the edge property under the open boundary condition, and the winding number (the bulk topological invariant), we find that these interesting long-rang hoppings generate nontrivial topological superradiant phases, especially with the winding number $\mathcal{W} = -1$ and two edge states, and the winding number $\mathcal{W} = 2$ and four edge states (without shaking, the topological superradiant phase only with the winding number $\mathcal{W} = 1$ and two edge states can be found [27,28]). Finally, we briefly address possible experiment observations of the predicted topological superradiant phases. Our results provide another way to explore novel many-body physics in cavity quantum electrodynamics systems.

II. MODEL AND HAMILTONIAN

We consider an ensemble of Fermi atoms in a cavity-mode-induced shaken optical lattice. As shown in Fig. 1(a), all fermions are trapped in a quasi-one-dimensional background optical lattice along the cavity axis $\hat{x}$, which can be prepared by a strong confinement in the other directions. These fermions are not only coupled to a cavity mode with a linearly polarized driving along the cavity axis $\hat{x}$, but also pumped by a linearly polarized laser along the $\hat{z}$ direction. Two electro-optic modulators are placed in the optical cavity and can be used for controlling the phase of cavity mode

*chengang971@163.com

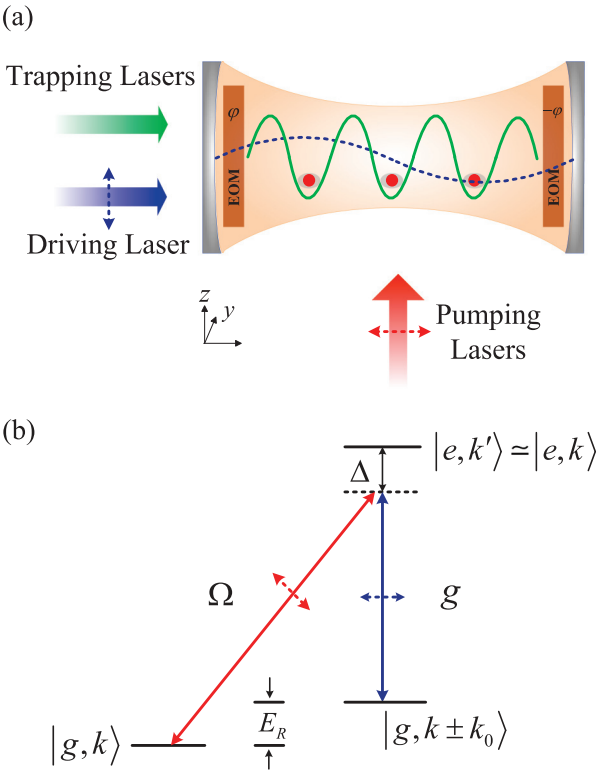

FIG. 1. (a) Proposed schematic setup. Fermions are loaded in a background optical lattice (green solid curve) inside an optical cavity and are also pumped by a transverse laser. The linearly polarized cavity mode (blue dashed curve) is shaken by two electro-optic modulators (EOMs). (b) The coupling of momentum states and their transitions via the pump and cavity fields. The definition of different labels can be seen in the main text.

and the background potential via varying potential voltage on the introduced two electro-optic modulators at the same time. In this case, the cavity mode becomes shaking and its amplitude can be written as $E \propto \cos[k_0 x + \varphi(t)]$, where k_0 is the wave number and $\varphi(t) = \varphi_0 + \chi\cos(\omega t)$ is the time-dependent phase with χ being the strength of the shaken term, φ_0 being the relative phase between the background lattice and the cavity field, and ω being the frequency of the applied potential voltage. When ω is larger than the free spectral range of an optical cavity, the electro-optic modulators can slowly modify the optical phase [46]. Since the optical path length is not affected by the two electro-optic modulators, the resonant frequency of the cavity is not changed.

On the other hand, each fermion contains two energy levels, the ground and excited states labeled respectively as $|g\rangle$ and $|e\rangle$. For a sufficiently strong confinement in the transverse direction, the atomic motion is restricted to one dimension along the cavity axis $\hat{x}$ and suffers a recoil momentum k_0 from photons in the cavity mode. As a result, the energy levels can be expressed effectively by two ground states ($|g,k\rangle$ and $|g,k\pm k_0\rangle$) and one excited state ($|e,k'\rangle \simeq |e,k\rangle$), where k is the atomic momentum, and moreover, these ground states are separated by the recoil energy $E_R = \hbar^2 k_0^2/(2m)$. The pumping laser couples the states $|g,k\rangle$ and $|e,k\rangle$ with the Rabi frequency Ω, whereas the cavity field governs the transition between the states $|g,k\pm k_0\rangle$ and $|e,k\rangle$ with $g = g_0\cos[k_0 x + \varphi(t)]$ being the shaken atom-photon coupling strength, as shown in Fig. 1(b). The pumping frequency ω_p is close to the cavity frequency ω_c, both of which are detuned far from the atomic transition frequency ω_a.

When $|\Delta| \equiv |\omega_p - \omega_a| \gg \{g,\Omega\}$, the excited state of fermions can be adiabatically eliminated and the system can be described by a time-dependent Hamiltonian

$$\hat{H}(t) = \int dx\hat{\psi}^\dagger(x)\Big\{\frac{p_x^2}{2m} + V_0\cos^2[k_0x + \chi\cos(\omega t)] + U\hat{a}^\dagger\hat{a}\cos^2[k_0x+\varphi(t)] + \eta(\hat{a}^\dagger+\hat{a})\cos[k_0x+\varphi(t)]\Big\}\hat{\psi}(x) - \Delta_c\hat{a}^\dagger\hat{a}, \quad (1)$$

where $\hat{\psi}(x)$ is the one-dimensional fermionic annihilation operator in the ground state, $\hat{a}$ is the annihilation operator of the quantized cavity field with $\Delta_c = \omega_p - \omega_c$ being the detuning, m is the atomic mass, V_0 is the background lattice depth, $U = g^2/\Delta$ is the optical potential depth per photon, $\eta = g\Omega/\Delta$ is the effective pump strength, and N is the total number of atoms.

The Hamiltonian (1) shows that the shaking of the cavity field generates a time-dependent dynamical optical lattice, $U\hat{a}^\dagger\hat{a}\cos^2[k_0x+\varphi(t)]$. When the cavity field is cohered, the atoms self-organize into an effective time-dependent optical lattice that is bound by the interference term in the Hamiltonian (1). This in turn affects the light scattering into the cavity (i.e., the amplitude of the shaken optical lattice) and starts a self-consistent process. When the cavity field is suppressed, the shaking disappears and the self-consistent process is prohibited. These are quite different from the previous studies about the shaken optical lattices without backaction on the atomic degrees of freedom [30,34–37,42], and will generate new quantum states with exotic properties. For simplicity, in the following we choose red detuning for the cavity ($\Delta_c < 0$) and blue detuning for fermions ($\Delta > 0$).

By transferring to the comoving frame, $x \to x - x(t)$, where $x(t) = \chi\cos(\omega t)/k_0$ is the periodic trajectory [34], the Hamiltonian (1) can be written as

$$\hat{H}(t) = \int dx\hat{\psi}^\dagger(x)\Big\{\frac{p_x^2}{2m} + V_0\cos^2(k_0x) + U\hat{a}^\dagger\hat{a}\cos^2(k_0x+\varphi_0) + \frac{K_0x}{d}\cos(\omega t) + \eta(\hat{a}^\dagger+\hat{a})\cos(k_0x+\varphi_0)\Big\}\hat{\psi}(x) - \Delta_c\hat{a}^\dagger\hat{a}, \quad (2)$$

where $K_0 = dm\chi\omega^2/k_0$ with $d = \pi/k_0$ being the lattice constant.

Here we consider a deep background lattice (i.e., $|V_0| \gg U\langle\hat{a}^\dagger\hat{a}\rangle$), in which the atomic field operator $\hat{\psi}(x)$ can be expanded as the lowest-band Wannier functions $W(x-x_i)$ of the background lattice potential [1], i.e.,

$$\hat{\psi}(x) = \sum_i \hat{b}_i W(x-x_i), \quad (3)$$

where $\hat{b}_i$ denotes the atomic annihilation operator of the ith site [19]. In this case, the Hamiltonian (2) is transformed into

a single-band Hamiltonian

$$\hat{H}_{\rm lat}(t) = -\tilde{\Delta}_c \hat{a}^\dagger \hat{a} + \frac{K_0}{d}\cos(\omega t)\sum_i x_i \hat{b}_i^\dagger \hat{b}_i + \sum_{i,j>0}[t_{i,i\pm j} + \eta(\hat{a}^\dagger + \hat{a})M_{i,i\pm j}]\hat{b}_i^\dagger \hat{b}_{i\pm j}. \quad (4)$$

Here $\tilde{\Delta}_c = \Delta_c - UNM_0$ is the effective cavity detuning with UNM_0 being the dispersive shift of the cavity, where $M_0 = \int dx W^*(x - x_i)\cos^2(k_0 x + \varphi_0)W(x - x_i)$. The lattice and Raman-induced hopping coefficients are given respectively by

$$t_{i,i\pm j} = \int dx W^*(x - x_i)\left[\frac{p_x^2}{2m} + V_0\cos^2(k_0 x)\right]W(x - x_{i\pm j}), \quad (5)$$

$$M_{i,i\pm j} = \int dx W^*(x - x_i)\cos(k_0 x + \varphi_0)W(x - x_{i\pm j}). \quad (6)$$

The fully theoretical treatment for the time-dependent Hamiltonian (4) is based on the Floquet theory. Usually, according to the scenario of the shaken optical lattice [29], this time-dependent Hamiltonian is transformed into a time-independent term. Specially, we perform a unitary transformation

$$\hat{U}(t) = \exp\left\{i\sum_j\left[\frac{K}{d}\sin(\omega t)x_j\right]\hat{b}_j^\dagger \hat{b}_j\right\}, \quad (7)$$

where $K = K_0/\omega = dm\chi\omega/k_0$. Then using the Bessel function expansion $\exp[iK\sin(\omega t)] = \sum_{n=-\infty}^{n=\infty} J_n(K)\exp(in\omega t)$ and applying the rotating-wave-type approximation (i.e., $\omega \gg \{g, \Omega, \Delta_c\}$) [29], the Hamiltonian (4) is written in its cycle average as

$$\hat{H}_{\rm eff} = \frac{1}{T}\int dt \hat{H}_{\rm lat}(t) = -\tilde{\Delta}_c \hat{a}^\dagger \hat{a} + \sum_{i,j>0} t_{i,i\pm j}J_0(jK)\hat{b}_i^\dagger \hat{b}_{i\pm j} + \eta(\hat{a}^\dagger + \hat{a})\sum_{i,j>0} J_0(jK)M_{i,i\pm j}\hat{b}_i^\dagger \hat{b}_{i\pm j}, \quad (8)$$

where $J_0(jK)$ is the zeroth-order Bessel function and $T = 2\pi/\omega$ is the time period.

In real experiments [2], the cavity decay usually exists. When considering this decay with the rate κ, we introduce the Heisenberg-Langevin equation for the cavity field operator $\hat{a}$. In general, the timescale of the atomic dynamics in the motion degree of freedom is larger than $1/\kappa$ on the timescale and then the cavity field can reach a steady state, i.e., $\partial\hat{a}/\partial t = 0$ [1]. This leads to a steady-state cavity field

$$\hat{a} = \sum_{i,j>0}\frac{\eta J_0(jK)M_{i,i\pm j}}{(\tilde{\Delta}_c + i\kappa)}\hat{b}_i^\dagger \hat{b}_{i\pm j}. \quad (9)$$

Substituting Eq. (9) into the Hamiltonian (8) and then adopting the mean-field approach on the cavity field, i.e., $\alpha = \langle\hat{a}\rangle/\sqrt{N}$, the Hamiltonian (8) becomes

$$\hat{H}_{\rm eff} = -\frac{N(\tilde{\Delta}_c^2 + \kappa^2)}{4\tilde{\Delta}_c}\phi^2 + \sum_{i,j>0} t_{i,i\pm j}J_0(jK)\hat{b}_i^\dagger \hat{b}_{i\pm j} + \eta\phi\sqrt{N}\sum_{i,j>0} J_0(jK)M_{i,i\pm j}\hat{b}_i^\dagger \hat{b}_{i\pm j}, \quad (10)$$

where the superradiant order parameter is defined as

$$\phi = \alpha + \alpha^* = \sum_{i,j>0}\frac{2\eta\tilde{\Delta}_c J_0(jK)M_{i,i\pm j}}{\sqrt{N}(\tilde{\Delta}_c^2 + \kappa^2)}\langle\hat{b}_i^\dagger \hat{b}_{i\pm j}\rangle. \quad (11)$$

The Hamiltonian (10) is still complicated and can be simplified as follows. For the background lattice potential, $V_0\cos^2(k_0 x)$, we have $t_{i,i\pm j} = (-1)^j t_j$. Notice that the potential induced by the cavity mode, $\eta\phi\cos(k_0 x + \varphi_0)$, has twice the period of the background lattice potential, the atomic detuning is blue, and dimerization is homopolar (zero offset) [47]. Thus we find $M_{i,i\pm(2j-1)} = \pm(-1)^i M_{2j-1}$ and $M_{i,i\pm 2j} = 0$. On the other hand, since here we only consider the deep background lattice, the dominate hopping coefficients $t_{i,j}$ can be described by an asymptotic law [48,49], i.e., $t_{i,j} \sim (x_{i,j})^{-3/2}e^{-hx_{i,j}}$ with $x_{i,j}$ being the interval between two different lattice sites and h being the distance of a branch point from the real axis in the complex momentum space. For the deep-well case, $h/k_0 \sim \sqrt{V_0/(4E_R)} - 1/4$, which becomes $h/k_0 \sim V_0/(8E_R)$ in the weak-binding case. When the parameter V_0/E_R is decreased, the long-range hoppings occur. For example, if $V_0/E_R = 3.5$, we numerically obtain $t_{i,i\pm 2}/t_{i,i\pm 1} \sim 0.1$, $t_{i,i\pm 3}/t_{i,i\pm 1} \sim 0.01$, $t_{i,i\pm 4}/t_{i,i\pm 1} \sim 0.001$, and $M_{i,i\pm 3}/M_{i,i\pm 1} \sim 0.02$. These mean that we only consider the NN, NNN, and NNNN hopping terms to ensure the reliability of the results in our work; i.e., the Hamiltonian (10) is rewritten as

$$\hat{H}_{\rm eff} = -\frac{\tilde{\Delta}_c^2 + \kappa^2}{4\tilde{\Delta}_c}\phi^2 N + \upsilon_1 J_0(K)\sum_{m=1}\hat{b}_{m,A}^\dagger \hat{b}_{m,B} + w_1 J_0(K)\sum_{m=1}\hat{b}_{m,B}^\dagger \hat{b}_{m+1,A} + \upsilon_2 J_0(2K)\sum_{m=1}\hat{b}_{m,A}^\dagger \hat{b}_{m+1,A} + w_2 J_0(2K)\sum_{m=1}\hat{b}_{m,B}^\dagger \hat{b}_{m+1,B} + \upsilon_3 J_0(3K)\sum_{m=1}\hat{b}_{m,A}^\dagger \hat{b}_{m+1,B} + w_3 J_0(3K)\sum_{m=1}\hat{b}_{m,B}^\dagger \hat{b}_{m+2,A} + \text{H.c.}, \quad (12)$$

where A and B are two different sites in one unit cell m, H.c. is the Hermitian conjugate, and the effective hopping coefficients are given respectively by

$$\upsilon_1 = t_1 + \eta\phi M_1\sqrt{N}, \quad w_1 = t_1 - \eta\phi M_1\sqrt{N}, \quad (13)$$

$$\upsilon_2 = w_2 = -t_2, \quad (14)$$

$$\upsilon_3 = t_3 + \eta\phi M_3\sqrt{N}, \quad w_3 = t_3 - \eta\phi M_3\sqrt{N}. \quad (15)$$

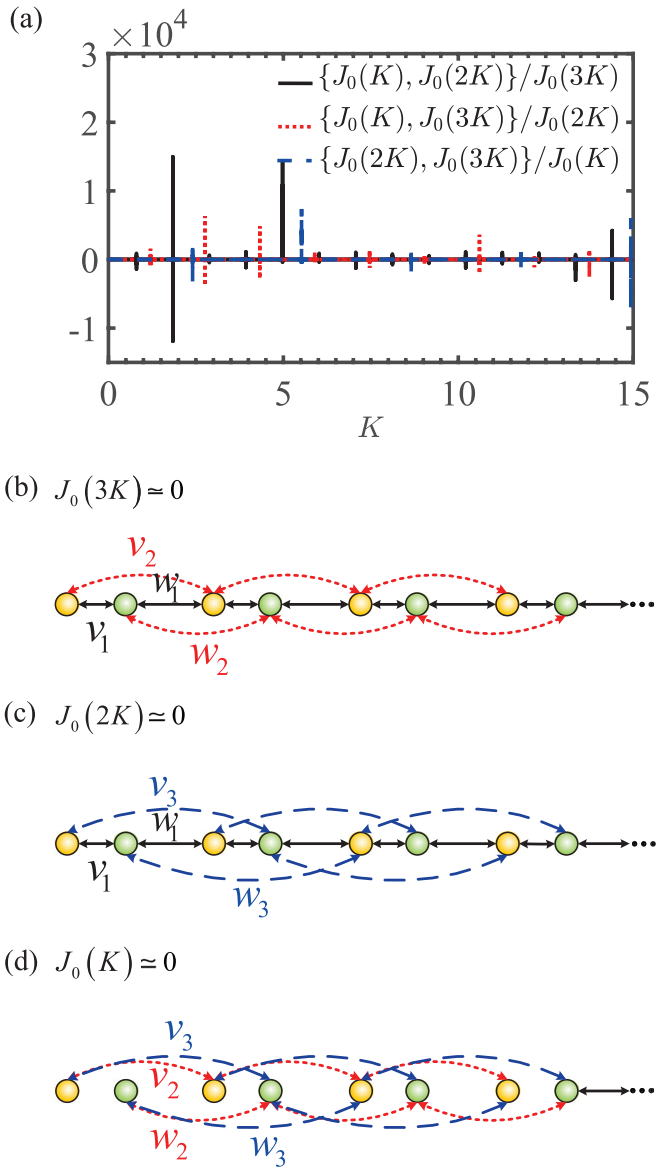

FIG. 2. (a) The different ratios of the zeroth-order Bessel functions. The black solid, red dotted, and blue dashed curves reflect the ratios of $\{J_0(K), J_0(2K)\}/J_0(3K)$, $\{J_0(K), J_0(3K)\}/J_0(2K)$, and $\{J_0(2K), J_0(3K)\}/J_0(K)$, respectively. (b)–(d) The different hopping situations of (b) $J_0(3K) \simeq 0$, (c) $J_0(2K) \simeq 0$, and (d) $J_0(K) \simeq 0$. $\{v_1, w_1\}$, $\{v_2, w_2\}$, and $\{v_3, w_3\}$ are the NN, NNN, and NNNN hopping coefficients, respectively.

In contrast to the previous cases [42], the hopping coefficients achieved here are dependent on the cavity field. They can be tuned independently through varying the shaken strength χ and the shaken frequency ω in the zeroth-order Bessel functions. As shown by the black solid curves in Fig. 2(a), when $K = 0.801(2), 1.84, 2.884(5)\ldots$, $\{J_0(K), J_0(2K)\} \gg J_0(3K)$ and the NN and NNN hoppings are preserved [see Fig. 2(b)]. When $K = 1.202(3), 2.76, 4.327\ldots$ [red dotted curves in Fig. 2(a)], $\{J_0(K), J_0(3K)\} \gg J_0(2K)$ and only the NNN hopping is obviated [see Fig. 2(c)]. When $K = 2.405, 5.52, 8.654\ldots$ [blue dashed curves in Fig. 2(a)], $\{J_0(2K), J_0(3K)\} \gg J_0(K)$ and both NNN and NNNN hoppings exist, but the conventional NN hopping disappears [see Fig. 2(d)]. This case shares the pure long-range character. These different situations may exhibit rich physics. As an example, here we will reveal nontrivial topological superradiant phases. In the following, $|\upsilon_2|$ is set as the energy unit.

III. TOPOLOGICAL SUPERRADIANT PHASES

Since the hopping coefficients in Eqs. (13) and (15) depend crucially on the cavity field ϕ arising from the collective excitation of the system in the thermodynamic limit, the topological properties of the Hamiltonian (12) should be obtained by self-consistently solving Eq. (11). To solve this equation, we define the free energy as

$$F = -\frac{N(\tilde{\Delta}_c^2 + \kappa^2)}{4\tilde{\Delta}_c}\phi^2 + \langle \hat{H}_a \rangle, \tag{16}$$

where $\hat{H}_a$ is the Hamiltonian of the atomic system in the Hamiltonian (12). According to $\langle \hat{H}_a \rangle \simeq E_{fb}$ with E_{fb} being the energy band obtained from the Hamiltonian $\hat{H}_a$, the free energy becomes

$$F = -\frac{N(\tilde{\Delta}_c^2 + \kappa^2)}{4\tilde{\Delta}_c}\phi^2 + E_{fb}. \tag{17}$$

Using the Hellman-Feynman theorem, $\partial\langle \hat{H}_a \rangle/\partial\phi = \partial E_{fb}/\partial\phi$, where $\partial\langle \hat{H}_a \rangle/\partial\phi = \eta\sqrt{N}\sum_{i,j>0} J_0(jK) M_{i,i\pm j}\langle \hat{b}_i^\dagger \hat{b}_{i\pm j}\rangle$ derived from the Hamiltonian (10), the extremum of the free energy, $\partial F/\partial\phi = 0$, leads to the same result in Eq. (11). This means that the self-consistent solution of the cavity field can be obtained directly by finding the stationary point of the free energy. In addition, to fully determine the steady-state solutions, the stability condition, $\partial^2 F/\partial\phi^2 > 0$, should also be taken into account.

To study topological properties of the Hamiltonian (12), we should analyze its bulk properties under the periodic boundary condition, the edge states under the open boundary condition, and the bulk topological invariant. For our considered one-dimensional system, the bulk topological invariant is governed by the winding number [50]

$$\mathcal{W} = \frac{1}{2\pi}\oint \frac{dk}{|\mathbf{h}(k)|^2}\{h_x(k)\partial_k[h_y(k)] - h_y(k)\partial_k[h_x(k)]\}. \tag{18}$$

The topological properties of the one-dimensional system can also be characterized by the Zak phase, which is the Berry phase obtained by the adiabatic motion of a particle across the Brillouin zone and is essentially a winding number of the direction of the motion [51].

A. NN and NNN (NNNN) hoppings

We first consider the case that $\{J_0(K), J_0(2K)\} \gg J_0(3K)$, in which the NN and NNN hoppings are preserved and the Hamiltonian (12) reduces to

$$\begin{aligned}\hat{H}_{eff} = &-\frac{N(\tilde{\Delta}_c^2 + \kappa^2)}{4\tilde{\Delta}_c}\phi^2 + \upsilon_1 J_0(K)\sum_{m=1}\hat{b}_{m,A}^\dagger \hat{b}_{m,B} \\ &+ w_1 J_0(K)\sum_{m=1}\hat{b}_{m,B}^\dagger \hat{b}_{m+1,A} + \upsilon_2 J_0(2K)\sum_{m=1}\hat{b}_{m,A}^\dagger \hat{b}_{m+1,A} \\ &+ w_2 J_0(2K)\sum_{m=1}\hat{b}_{m,B}^\dagger \hat{b}_{m+1,B} + \text{H.c.}\end{aligned} \tag{19}$$

TABLE I. Symmetries of the bulk Hamiltonians for different models. In the table, we denote the presence (absence) of the symmetry as ◯ (×).

Situations	Constraints on the Hamiltonians	Inversion Symmetry	Particle-Hole Symmetry	Chiral Symmetry
$J_0(3K) \simeq 0$	$\sigma_x H(k)\sigma_x = H(-k)$	◯	×	×
	$\sigma_x H(k)\sigma_x = H(-k)$			
$J_0(2K) \simeq 0$	$[\sigma_y H(k)\sigma_y]^* = -H(k)$	◯	◯	◯
	$\sigma_z H(k)\sigma_z = -H(k)$			
$J_0(K) \simeq 0$	$\sigma_x H(k)\sigma_x = H(-k)$	◯	×	×

In the Fourier space (i.e., the Bloch basis), $\hat{b}_{m,A} \propto \sum_k \exp(ikmd)\hat{b}_{kA}$ and $\hat{b}_{m,B} \propto \sum_k \exp(ikmd)\hat{b}_{kB}$ with $k \in [-k_0, k_0]$ (the first Brillouin zone), the bulk Hamiltonian

$$\hat{H}_{\text{bulk}}(k) = \sum_k \psi_k^\dagger [h_0(k)\mathcal{I} + h_x(k)\sigma_x + h_y(k)\sigma_y]\psi_k, \quad (20)$$

where $\psi_k = (\hat{b}_{kA}, \hat{b}_{kB})^T$, $\mathcal{I}$ is the unitary matrix, $h_0(k) = 2\upsilon_2 J_0(2K)\cos(kd)$, $h_x(k) = \upsilon_1 J_0(K) + w_1 J_0(K)\cos(kd)$, and $h_y(k) = w_1 J_0(K)\sin(kd)$. The bulk Hamiltonian (20) shows that in the presence of the NNN hopping, both the particle-hole and chiral symmetries are broken, but the inversion symmetry is preserved (see Table I).

The corresponding bulk eigenenergies

$$E_\pm = 2\upsilon_2 J_0(2K)\cos(kd) \pm \{[\upsilon_1 J_0(K)]^2 + [w_1 J_0(K)]^2 + 2\upsilon_1 w_1 J_0(K)^2 \cos(kd)\}^{\frac{1}{2}}. \quad (21)$$

In terms of Eq. (21), the extremum of the free energy ($\partial F/\partial\phi = 0$) leads to

$$\frac{N(\tilde{\Delta}_c^2 + \kappa^2)}{2\tilde{\Delta}_c}\phi - \sum_k \frac{\partial E_{k-}}{\partial\phi} = 0. \quad (22)$$

According to Eq. (22), in Fig. 3 we plot the cavity field ϕ with respect to the effective pump strength η_A, where $\eta_A = \eta M_1$. This figure shows that a small enough effective pump strength η_A can give rise to superradiance at zero temperature [52]. In addition, although the hopping coefficients in Eq. (13) depend crucially on the relative phase φ_0, the bulk eigenenergies $E_\pm$ are independent. As a result, the cavity field ϕ is also independent of the relative phase φ_0.

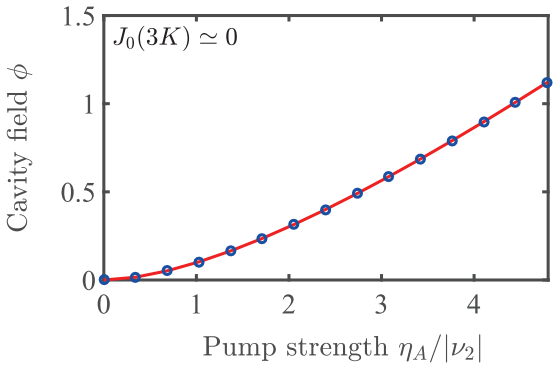

FIG. 3. The cavity field ϕ versus the effective pump strength η_A for the different relative phases $\varphi_0 = 0$ (red solid curve) and $\varphi_0 = \pi$ (blue open symbol) when $J_0(3K) \simeq 0$. The plotted parameters are $V_0/E_R = 3.5$, $\kappa/E_R = 1$, and $\tilde{\Delta}_c/E_R = -1$. The main properties for the other cases of $J_0(2K) \simeq 0$ and $J_0(K) \simeq 0$ are similar and thus not plotted here.

Having obtained the cavity field self-consistently, we can investigate the topological properties of the Hamiltonian (19). Only when the NN hopping exists, the system shares features of the photon-dependent Su-Schrieffer-Heeger (SSH)–Holstein model, which exhibits a nontrivial topological phase characterized by $\mathcal{W} = 1$ (the Zak phase $\varphi_{\text{Zak}} = \pi$) [28]. In the presence of the NNN hopping, in Fig. 4 we plot energy spectra of the bulk states under the periodic and open boundary conditions for the different cavity fields $\phi = 0$ and $\phi \neq 0$. When $\phi = 0$, the NN hopping coefficients become $\upsilon_1 = w_1 = t_1$, which are independent of the relative phase φ_0. In this case, the bulk gap is closed and the edge states always exist, as shown in Figs. 4(a1) and 4(b1). Thus the system is always in a gapless metallic phase. When $\phi \neq 0$, the results are quite different since the sign of the Raman-induced hopping coefficient M_1 in Eq. (6) depends crucially on the relative phase φ_0. For $\varphi_0 = 0$, $\cos(k_0 x + \varphi_0) = \cos(k_0 x)$ and thus $\upsilon_1 > w_1$. In this case, the bulk gap is open and there is no edge state in the superradiant-induced energy gap of a half-filled lattice with 80 sites [see Figs. 4(a2) and 4(b2)], and the system is in a superradiant insulator phase. For $\varphi_0 = \pi$, $\cos(k_0 x + \varphi_0) = -\cos(k_0 x)$ and thus $\upsilon_1 < w_1$. In such a case, the bulk gap is open and a pair of degenerate energy states emerge in the superradiant-induced energy gap, as shown in Figs. 4(a3) and 4(b3). The corresponding wave functions Φ are localized in the edges [insets of Fig. 4(b3)] and the system is in a nontrivial topological superradiant phase with $\mathcal{W} = 1$ ($\varphi_{\text{Zak}} = \pi$) also derived self-consistently from Eq. (18). These topological properties are similar to those of the photon-dependent SSH-Holstein model [28].

We now address briefly the case of $\{J_0(K), J_0(3K)\} \gg J_0(2K)$, in which the NN and NNNN hoppings are preserved. In this case, the inversion, particle-hole, and chiral symmetries are preserved (see Table I). As a result, the corresponding topological properties are also similar to those of the standard photon-dependent SSH-Holstein model [28] and are not listed here.

B. NNN and NNNN hoppings

Finally, we consider the case that $\{J_0(2K), J_0(3K)\} \gg J_0(K)$, in which both NNN and NNNN hoppings exist but the NN hopping disappears. In this case, the Hamiltonian (12) is

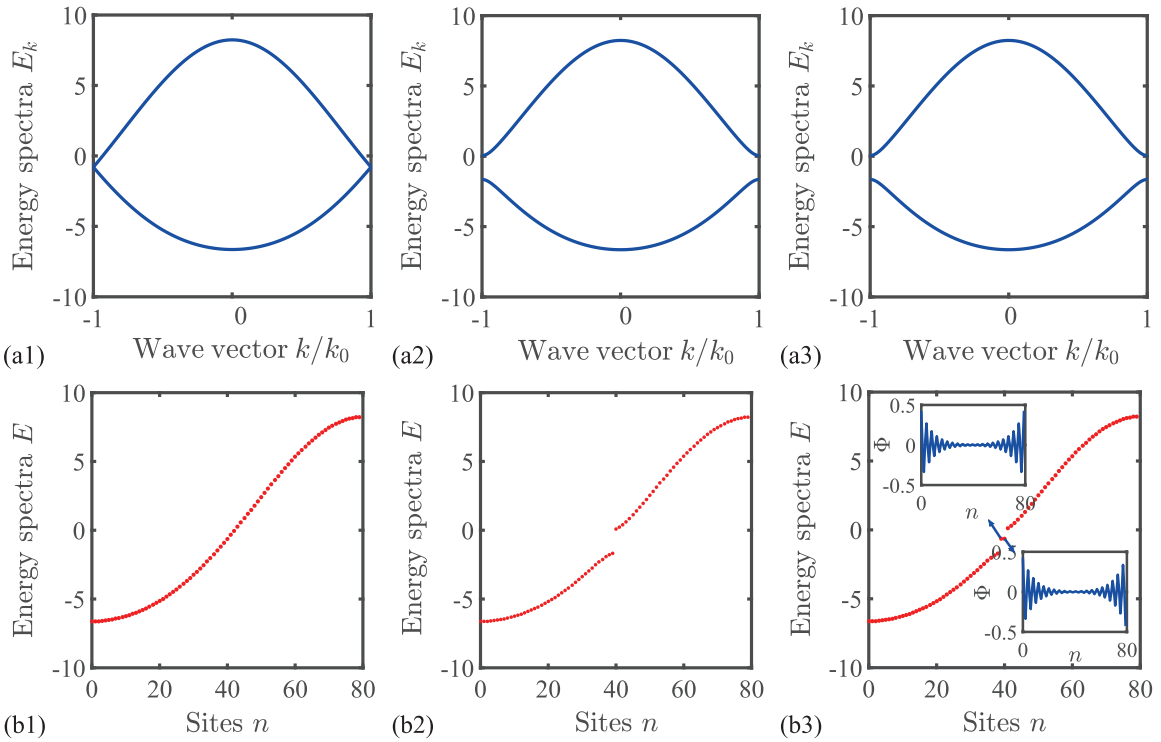

FIG. 4. The energy spectra of the bulk states for the periodic [(a1)–(a3)] and open [(b1)–(b3)] boundary conditions, when $\phi = 0$ [(a1), (b1)], $\phi = 0.50$ and $\varphi_0 = 0$ [(a2), (b2)], and $\phi = 0.50$ and $\varphi_0 = \pi$ [(a3), (b3)] with $\eta_A/E_R = 2.74$ and $K = 1.84$. The other parameters V_0/E_R, κ/E_R, and $\tilde{\Delta}_c/E_R$ are the same as those in Fig. 3. In (b1)–(b3), the half-filled lattice length is chosen as 80 sites. Insets of (b3): Localized wave functions Φ of the edge modes.

written as

$$\hat{H}_{\text{eff}} = -\frac{N\left(\tilde{\Delta}_c^2+\kappa^2\right)}{4\tilde{\Delta}_c}\phi^2 + \upsilon_2 J_0(2K)\sum_{m=1}\hat{b}^\dagger_{m,A}\hat{b}_{m+1,A} + w_2 J_0(2K)\sum_{m=1}\hat{b}^\dagger_{m,B}\hat{b}_{m+1,B} + \upsilon_3 J_0(3K)\sum_{m=1}\hat{b}^\dagger_{m,A}\hat{b}_{m+1,B} + w_3 J_0(3K)\sum_{m=1}\hat{b}^\dagger_{m,B}\hat{b}_{m+2,A} + \text{H.c.} \quad (23)$$

The bulk Hamiltonian

$$\hat{H}_{\text{bulk}}(k) = \sum_k \psi_k^\dagger[h_0(k)\mathcal{I} + h_x(k)\sigma_x + h_y(k)\sigma_y]\psi_k, \quad (24)$$

where $h_0(k) = 2\upsilon_2 J_0(2K)\cos(kd)$, $h_x(k) = \upsilon_3 J_0(3K)\cos(kd) + w_3 J_0(3K)\cos(2kd)$, and $h_y(k) = -\upsilon_3 J_0(3K)\sin(kd) + w_3 J_0(3K)\sin(2kd)$. The bulk Hamiltonian (23) shows that in the presence of the NNN hopping, both the particle-hole and chiral symmetries are broken, but the inversion symmetry is preserved (see Table I), which is the same as the situation of $J_0(3K) \simeq 0$. The corresponding bulk eigenenergies

$$E_\pm = 2\upsilon_2 J_0(2K)\cos(kd) \pm \{[\upsilon_3 J_0(3K)]^2 + [w_3 J_0(3K)]^2 + 2\upsilon_3 w_3 [J_0(3K)]^2\cos(3kd)\}^{\frac{1}{2}}. \quad (25)$$

In Fig. 5, we plot the energy spectra of the bulk states under the period and open boundary conditions for the different cavity fields $\phi = 0$ and $\phi \neq 0$. When $\phi = 0$, the staggered NNNN hopping coefficients become $\upsilon_3 = w_3 = t_3$ and are independent of the relative phase φ_0. In this case, the bulk gap is closed and the edge states always exist, as shown in Figs. 5(a1) and 5(b1). The system is always in a metallic phase. When $\phi \neq 0$, the staggered NNNN hopping coefficients υ_3 and w_3 are related to the Raman-induced hopping coefficient M_3 and are thus dependent on the relative phase φ_0. For $\varphi_0 = 0$, we have $\upsilon_3 > w_3$. In this case, the bulk gap is open and there are two degenerate energy states in the superradiant-induced gap, as shown in Figs. 5(a2) and 5(b2). The corresponding wave functions Φ are localized in the edges [insets of Fig. 5(b2)]. From the bulk Hamiltonian (24), we find that $\upsilon_3 J_0(3K)\cos(kd)$ and $-\upsilon_3 J_0(3K)\sin(kd)$ play dominant roles in the vector $\mathbf{h}(k)$ and then the end point of the vector $\mathbf{h}(k)$ traces out a closed loop, including a singular point with k going across the Brillouin zone. The system is in a nontrivial topological superradiant phase with $\mathcal{W} = -1$ ($\varphi_{\text{Zak}} = -\pi$). Interestingly, for $\phi \neq 0$, we have $\upsilon_3 < w_3$. In such a case, the bulk gap is open and there exist four degenerate energy states in the superradiant-induced gap, as shown in Figs. 5(a3) and 5(b3). Edges host four localized wave functions Φ, as shown in Fig. 6. From the bulk Hamiltonian (24), $w_3 J_0(3K)\cos(2kd)$ and $w_3 J_0(3K)\sin(2kd)$ play dominant roles in the vector $\mathbf{h}(k)$ and the end point of the vector $\mathbf{h}(k)$ traces out two closed loops, including a singular point with k going across the Brillouin zone. The system is in a nontrivial topological superradiant phase with $\mathcal{W} = 2$ ($\varphi_{\text{Zak}} = 2\pi$). The presence of the NNNN hopping enriches the topological properties, which are quite different from those in the photon-dependent SSH-Holstein model [28].

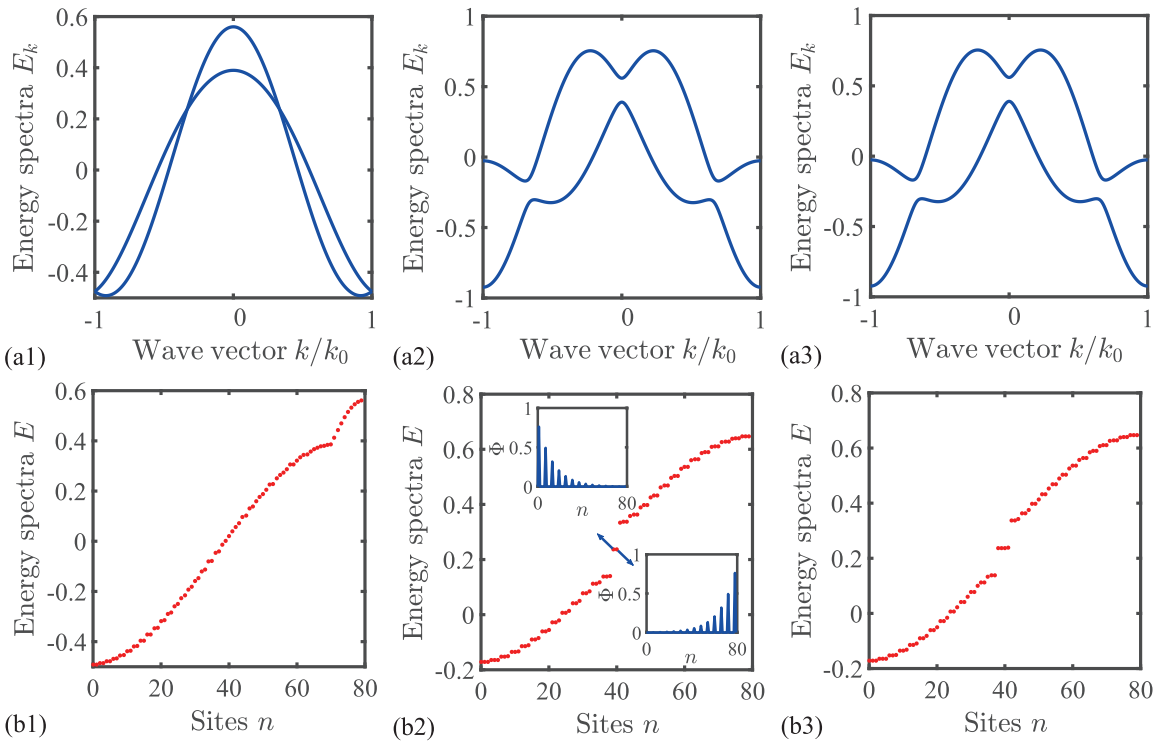

FIG. 5. The energy spectra of the bulk states for the periodic [(a1)–(a3)] and open [(b1)–(b3)] boundary conditions, when $\phi = 0$ [(a1), (b1)], $\phi = 0.43$ and $\varphi_0 = 0$ [(a2), (b2)], and $\phi = 0.43$ and $\varphi_0 = \pi$ [(a3), (b3)] with $\eta_A/E_R = 1.43$ and $K = 2.405$. The other parameters V_0/E_R, κ/E_R, and $\tilde{\Delta}_c/E_R$ are the same as those in Fig. 3. In (b1)–(b3), the half-filled lattice length is chosen as 80 sites. Insets of (b2): Wave functions Φ of the edge modes.

IV. PARAMETER ESTIMATION AND POSSIBLE EXPERIMENTAL OBSERVATION

In this section, we take the ^{6}Li atom as an example to estimate the related parameters and address briefly how to detect the predicted topological superradiant phases. For the fermionic ^{6}Li atoms, we estimate the recoil energy $E_R \sim 20$ kHz, and set $V_0 = 3.5E_R$, $g \sim 58$ kHz (by varying the frequency of the linearly polarized driving laser), $\Delta \sim 5$ MHz, $\kappa \sim 20$ kHz, and $\Delta_c \sim -6$ kHz. When the total number of atoms with $N = 80$ is fixed, $UNM_0 \sim 14$ kHz and thus $\tilde{\Delta}_c \sim 20$ kHz. Based on these estimated parameters, the single-band approximation in deriving the Hamiltonian (4) and the steady-state condition for cavity field are feasible. On the other hand, for one dimension, the filling factor $\nu = \bar{n}/(2k_0)$ [53], where $\bar{n}$ is the average density of the Fermi atoms. The half filling can be in principle achieved experimentally by controlling $\bar{n}$ through varying the total atom number, the lattice depth, or the evaporation parameters [53], and can also be directly measured by using the on-site number-sensitive quantum gas microscope [54].

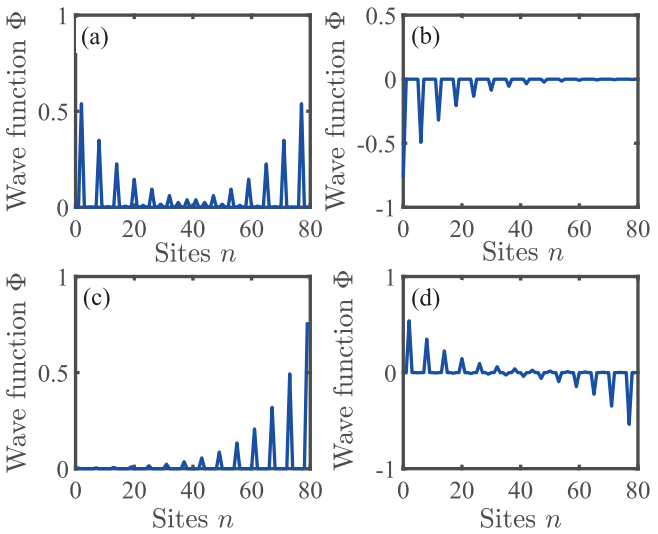

FIG. 6. The localized wave functions Φ for four degenerate edge states in Fig. 5(b3).

The shaken-cavity mode can be realized by two electro-optic modulators that are placed in the optical cavity. The optical phase can be modified by tuning the applied voltage. According to the experimental scheme [55], a high-finesse cavity with a loss rate $\kappa \lesssim 100$ kHz can be realized by using high-reflection mirrors. The relative phase φ_0 can be tuned to the relative position between the background lattice and the cavity field. Using the high-efficiency antireflection coating [56] and low-absorption electro-optic materials [57], the electro-optic modulators inside the cavity can have low losses. Then the strength of the shaken term is small $\chi \sim 0.1\pi$ and the frequency of the applied potential voltage ω is of several hundred kHz. Under the above parameters, the rotating-wave-type approximation in deriving the Hamiltonian (8) can also be applied.

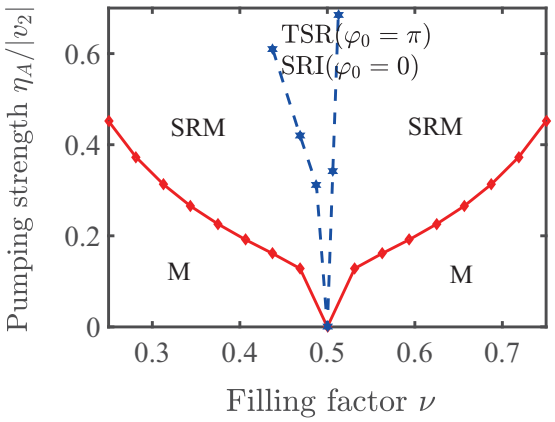

FIG. 7. Phase diagram in the η_A-ν plane when $J_0(3K) \simeq 0$. The other parameters V_0, κ, and $\tilde{\Delta}_c$ are the same as those in Fig. 3. The abbreviations of M, SRM, TSR, and SRI denote metallic, superradiant metallic, topological superradiant, and superradiant insulator, respectively. Around the half filling ($\nu = 0.5$), there exists a phase transition between the M phase and the TSR ($\varphi_0 = \pi$) and SRI ($\varphi_0 = 0$) phases. Away from the half filling, the system is in a gapless SRM phase.

Finally, we briefly address how to detect the predicted topological superradiant phases, which are mainly governed by the scaled cavity field ϕ, the topological invariant, and the edge states. In experiments, the cavity field ϕ can be detected using calibrated single-photon counting modules [2]. The topological invariant can be measured directly by the Bloch-Ramsey interferometric technique [58], and the degenerate edge states in the nontrivial topological superradiant phases can be observed in the spectral properties of the cavity output [28]. Based on these developed experimental techniques, we believe that the predicted nontrivial topological superradiant phase could be detected in experiments.

V. DISCUSSION AND CONCLUSIONS

Before ending this paper, we make one remark. In the above discussion, the filling factor is restricted to $\nu = 0.5$ (half filling), which is however difficult to realize accurately in experiments. In Fig. 7, we plot the phase diagram versus the effective pump strength η_A and the filling factor ν for $J_0(3K) \simeq 0$. This figure shows that around half filling, the system is either a topological superradiant phase ($\varphi_0 = \pi$) or a superradiant insulator phase ($\varphi_0 = 0$). This result benefits for observing the predicted topological superradiant phase in real experiments. There also exists a phase transition between the metallic phase and the topological superradiant ($\varphi_0 = \pi$) or superradiant insulator ($\varphi_0 = 0$) phases, while away from half filling, the system is in a gapless superradiant metallic phase. When $J_0(K) \simeq 0$, the main phase diagram is similar to that of $J_0(3K) \simeq 0$. A slight difference is that for $\varphi_0 = \pi$, the topological superradiant phase with $W = 1$ is replaced by that with $W = 2$, while for $\varphi_0 = 0$, the superradiant insulator phase is replaced by the topological superradiant phase with $W = -1$. Thus, the phase diagram in this case is not plotted here.

In summary, we have proposed a quantum manipulation for the hopping amplitudes through the cavity scheme and studied the corresponding nontrivial topological properties. Specifically, we have considered the steady state of Fermi atoms coupled to a shaken cavity field at half filling. This shaking generates a time-dependent dynamical optical lattice with backaction on the atomic degrees of freedom. In the high-frequency limit, the shaken dynamical optical lattice generates the cavity-field-dependent long-range hoppings with high controllability. These interesting long-range hoppings produce nontrivial topological superradiant phases, especially with a large winding number and four degenerate edge states, which are quite different from those without shaking [27,28] . Finally, we have also briefly addressed possible experimental observations of the predicted nontrivial topological superradiant phases. Our results provide another way to explore novel many-body physics in cavity quantum electrodynamics systems.

ACKNOWLEDGMENTS

This work is supported partly by the National Key R&D Program of China under Grant No. 2017YFA0304203, the NSFC under Grants No. 11674200 and No. 11804204, and 1331KYC.

[1] H. Ritsch, P. Domokos, F. Brennecke, and T. Esslinger, Rev. Mod. Phys. **85**, 553 (2013).
[2] K. Baumann, C. Guerlin, F. Brennecke, and T. Esslinger, Nature (London) **464**, 1301 (2010).
[3] J. Léonard, A. Morales, P. Zupancic, T. Esslinger, and T. Donner, Nature (London) **543**, 87 (2017).
[4] J. Léonard, A. Morales, P. Zupancic, T. Donner, and T. Esslinger, Science **358**, 1415 (2017).
[5] Y. Deng, J. Cheng, H. Jing, and S. Yi, Phys. Rev. Lett. **112**, 143007 (2014).
[6] W. Zheng and N. R. Cooper, Phys. Rev. Lett. **117**, 175302 (2016).
[7] C. Kollath, A. Sheikhan, S. Wolff, and F. Brennecke, Phys. Rev. Lett. **116**, 060401 (2016).
[8] A. Sheikhan, F. Brennecke, and C. Kollath, Phys. Rev. A **93**, 043609 (2016).
[9] C.-M. Halati, A. Sheikhan, and C. Kollath, Phys. Rev. A **96**, 063621 (2017).
[10] A. Sheikhan, F. Brennecke, and C. Kollath, Phys. Rev. A **94**, 061603(R) (2016).
[11] K. E. Ballantine, B. L. Lev, and J. Keeling, Phys. Rev. Lett. **118**, 045302 (2017).
[12] D. González-Cuadra, P. R. Grzybowski, A. Dauphin, and M. Lewenstein, Phys. Rev. Lett. **121**, 090402 (2018).
[13] C. Georges, J. G. Cosme, L. Mathey, and A. Hemmerich, Phys. Rev. Lett. **121**, 220405 (2018).
[14] G. Kónya, D. Nagy, G. Szirmai, and P. Domokos, Phys. Rev. A **98**, 063608 (2018).

[15] R. Mottl, F. Brennecke, K. Baumann, R. Landig, T. Donner, and T. Esslinger, Science **336**, 1570 (2012).
[16] J. Klinder, H. Kessler, M. R. Bakhtiari, M. Thorwart, and A. Hemmerich, Phys. Rev. Lett. **115**, 230403 (2015).
[17] S. F. Caballero-Benitez and I. B. Mekhov, Phys. Rev. Lett. **115**, 243604 (2015).
[18] M. R. Bakhtiari, A. Hemmerich, H. Ritsch, and M. Thorwart, Phys. Rev. Lett. **114**, 123601 (2015).
[19] R. Landig, L. Hruby, N. Dogra, M. Landini, R. Mottl, T. Donner, and T. Esslinger, Nature (London) **532**, 476 (2016).
[20] N. Dogra, F. Brennecke, S. D. Huber, and T. Donner, Phys. Rev. A **94**, 023632 (2016).
[21] Y. Chen, Z. Yu, and H. Zhai, Phys. Rev. A **93**, 041601(R) (2016).
[22] T. Flottat, L. de Forges de Parny, F. Hébert, V. G. Rousseau, and G. G. Batrouni, Phys. Rev. B **95**, 144501 (2017).
[23] L. Hruby, N. Dogra, M. Landini, T. Donner, and T. Esslinger, Proc. Natl. Acad. Sci. USA **115**, 3279 (2018).
[24] J. Panas, A. Kauch, and K. Byczuk, Phys. Rev. B **95**, 115105 (2017).
[25] J. Fan, X. Zhou, W. Zheng, W. Yi, G. Chen, and S. Jia, Phys. Rev. A **98**, 043613 (2018).
[26] F. Mivehvar, H. Ritsch, and F. Piazza, Phys. Rev. Lett. **122**, 113603 (2018).
[27] J.-S. Pan, X.-J. Liu, W. Zhang, W. Yi, and G.-C. Guo, Phys. Rev. Lett. **115**, 045303 (2015).
[28] F. Mivehvar, H. Ritsch, and F. Piazza, Phys. Rev. Lett. **118**, 073602 (2017).
[29] A. Eckardt, Rev. Mod. Phys. **89**, 011004 (2017).
[30] H. Lignier, C. Sias, D. Ciampini, Y. Singh, A. Zenesini, O. Morsch, and E. Arimondo, Phys. Rev. Lett. **99**, 220403 (2007).
[31] V. V. Ivanov, A. Alberti, M. Schioppo, G. Ferrari, M. Artoni, M. L. Chiofalo, and G. M. Tino, Phys. Rev. Lett. **100**, 043602 (2008).
[32] C. Sias, H. Lignier, Y. P. Singh, A. Zenesini, D. Ciampini, O. Morsch, and E. Arimondo, Phys. Rev. Lett. **100**, 040404 (2008).
[33] A. Alberti, V. V. Ivanov, G. M. Tino, and G. Ferrari, Nat. Phys. **5**, 547 (2009).
[34] J. Struck, C. Ölschläger, R. Le Targat, P. Soltan-Panahi, A. Eckardt, M. Lewenstein, P. Windpassinger, and K. Sengstock, Science **333**, 996 (2011).
[35] C. V. Parker, L. C. Ha, and C. Chin, Nat. Phys. **9**, 769 (2013).
[36] W. Zheng, B. Liu, J. Miao, C. Chin, and H. Zhai, Phys. Rev. Lett. **113**, 155303 (2014).
[37] G. Jotzu, M. Messer, R. Desbuquois, M. Lebrat, T. Uehlinger, D. Greif, and T. Esslinger, Nature (London) **515**, 237 (2014).
[38] L.-C. Ha, L. W. Clark, C. V. Parker, B. M. Anderson, and C. Chin, Phys. Rev. Lett. **114**, 055301 (2015).
[39] C. J. Kennedy, W. C. Burton, W. C. Chung, and W. Ketterle, Nat. Phys. **11**, 859 (2015).
[40] M. Aidelsburger, M. Lohse, C. Schweizer, M. Atala, J. T. Barreiro, S. Nascimbene, N. R. Cooper, I. Bloch, and N. Goldman, Nat. Phys. **11**, 162 (2015).
[41] M. A. Khamehchi, C. Qu, M. E. Mossman, C. Zhang, and P. Engels, Nat. Commun. **7**, 10867 (2016).
[42] Z. Xu, Y. Zhang, and S. Chen, Phys. Rev. A **96**, 013606 (2017).
[43] M. Messer, K. Sandholzer, F. Görg, J. Minguzzi, R. Desbuquois, and T. Esslinger, Phys. Rev. Lett. **121**, 233603 (2018).
[44] N. Sun, P. F. Zhang, and H. Zhai, arXiv:1808.03966.
[45] X.-W. Luo and C. Zhang, Phys. Rev. Lett. **120**, 263202 (2018).
[46] A. Yariv and P. Yeh, *Photonics: Optical Electronics in Modern Communications* (Oxford Unversity Press, New York, 2007).
[47] F. Piazza and H. Ritsch, Phys. Rev. Lett. **115**, 163601 (2015).
[48] W. Kohn, Phys. Rev. **115**, 809 (1959).
[49] L. He and D. Vanderbilt, Phys. Rev. Lett. **86**, 5341 (2001).
[50] X. Li, E. Zhao, and W. V. Liu, Nat. Commun. **4**, 1523 (2013).
[51] J. Zak, Phys. Rev. Lett. **62**, 2747 (1989).
[52] Y. Chen, Z. Yu, and H. Zhai, Phys. Rev. Lett. **112**, 143004 (2014).
[53] I. Bloch, J. Dalibard, and W. Zwerger, Rev. Mod. Phys. **80**, 885 (2008).
[54] M. Boll, T. A. Hilker, G. Salomon, A. Omran, J. Nespolo, L. Pollet, I. Bloch, and C. Gross, Science **353**, 1257 (2016).
[55] B. Nagorny, T. Elsässer, and A. Hemmerich, Phys. Rev. Lett. **91**, 153003 (2003).
[56] H. K. Raut, V. A. Ganesh, A. S. Nair, and S. Ramakrishna, Energy Environ. Sci. **4**, 3779 (2011).
[57] M. Roth, N. Angert, M. Tseitlin, and A. Alexandrovski, Opt. Mater. **16**, 131 (2001).
[58] M. Atala, M. Aidelsburger, J. T. Barreiro, D. Abanin, T. Kitagawa, E. Demler, and I. Bloch, Nat. Phys. **9**, 795 (2013).